

Mode-Coupling Theory for Tagged-Particle Motion of Active Brownian Particles

Julian Reichert¹ and Thomas Voigtmann^{1,2}

¹*Institut für Materialphysik im Weltraum, Deutsches Zentrum für Luft- und Raumfahrt (DLR), 51170 Köln, Germany*

²*Department of Physics, Heinrich-Heine Universität Düsseldorf, Universitätsstr. 1, 40225 Düsseldorf, Germany*

(Dated: 2022-04-05)

We derive a mode-coupling theory (MCT) to describe the dynamics of tracer particles in dense, glass-forming systems of active Brownian particles (ABP) in two spatial dimensions. The ABP undergo translational and rotational Brownian dynamics, and are equipped with a fixed self-propulsion speed along their orientational vector that describes their active motility. The resulting equations of motion for the tagged-particle density correlation functions describe the various cases of tracer dynamics at high densities: that of a passive colloidal particle in a suspension of ABP, that of a single active particle in a glass-forming passive host suspensions, and that of active tracers in a bath of active particles. Numerical results are presented for these cases assuming hard-sphere interactions among the particles. The qualitative and quantitative accuracy of the theory is tested against event-driven Brownian-dynamics (ED-BD) simulations of active and passive hard disks. The agreement between simulation and theory is found to be excellent, provided one allows for an adjustment of overall density known from the fully passive system, and for a simple rescaling of self-propulsion velocities in the active host system. These adjustments account for the fact that ABP-MCT generally overestimates the tendency of kinetic arrest. We also confirm in the simulations a peculiar feature of the transient and stationary dynamical density correlation functions regarding their lack of symmetry under time reversal, demonstrating the non-equilibrium nature of the system and how it manifests itself in the theory.

I. INTRODUCTION

Systems of active Brownian particle (ABP) are paradigmatic models for non-equilibrium statistical physics. They are arguably the conceptually simplest toy model that incorporates thermalized random Brownian motion and non-equilibrium, active self-propelled motion typical of microswimmers, be they biological entities such as cells, micro-organisms, and the like, or be they artificial colloidal microswimmers such as suspended Janus particles driven by some energy field.

While a lot of attention has been devoted to the dilute and moderately dense active fluids, ABP also display intriguing features at high densities. If the corresponding passive system (in the absence of self-propulsion), is dense enough to form a (colloidal) glass, adding activity brings about interesting changes in the glass-transition behavior. For ABP, simulation studies [1] have demonstrated that an “active glass” state can be formed, at a density that shifts to higher densities when compared to the passive glass transition.

Theoretical studies of active glasses have so far mostly focused on a related model system, that of active Ornstein-Uhlenbeck particles (AOUP). The activity in this system is modeled through non-white noise, and in essence this provides for easier theoretical modeling as one does not have to take into account orientational degrees of freedom explicitly. Fewer studies address the dynamics of ABP at high densities.

In the present contribution, we extend our previous approach of using the mode-coupling theory of the glass transition (MCT) to describe the high-density dynamics of ABP [2, 3]. While the previous theory focused on the collective dynamics of density fluctuations near the

active-glass transition, here we complement that theory by equations of motion for the tagged-particle dynamical density correlation functions, to study tracer motion near the active- and passive-glass transition. Several points motivate this development: first, the tagged-particle dynamics is the observable that is most often studied in computer simulation of glass-forming systems, because of its better statistics. Second, many interesting physical effects arise from the interaction of active with passive particles. Third, the tagged-particle correlation functions provide the theoretical basis to derive also equations of motion for the mean-squared displacement (MSD) of tracer particles, which are the convenient observables to extract from the common experimental studies that investigate active suspensions by direct-imaging techniques.

A further central topic of the present paper is also to assess the accuracy of the mode-coupling theory for active Brownian particles (ABP-MCT) in comparison to computer simulation. To this end we employ event-driven Brownian dynamics (ED-BD) computer simulations [1, 4] as a tool to implement the dynamics of particles with strict hard-sphere no-overlap interactions.

The paper is structured as follows: in Sec. II we recapitulate the ABP-MCT for the collective dynamics, and extend it to include equations of motion for the tagged-particle dynamics of a tracer with possibly different interactions and different activity parameters than the host system. In Sec. III, we demonstrate numerical solutions of the equations of motion for the tracer-correlation functions, and compare the ABP-MCT results to those of our ED-BD simulations: after establishing the baseline in a comparison of passive-in-passive tracer dynamics, we turn to the motion of an active tracer first in the di-

lute system, then in the passive host system, and finally we discuss the motion of passive and active tracers in the dense active host system. Section IV provides concluding remarks.

II. THEORY

A. Mode-Coupling Theory

The ABP-MCT describes tagged-particle motion in ABP as coupled to the dynamics of collective density fluctuations; the corresponding equations for the latter have been derived by Liliashvili et al. [2] and shall be repeated here for completeness.

We study systems of N ABP in two spatial dimensions, with positions \vec{r}_k and orientation angles φ_k ($k = 1, \dots, N$). The stochastic equations of motion are

$$d\vec{r}_k = \mu \vec{F}_k dt + \sqrt{2D_t} d\vec{W}_k + v_0 \vec{n}(\varphi_k) dt, \quad (1a)$$

$$d\varphi_k = \sqrt{2D_r} dW_{\varphi_k}. \quad (1b)$$

Here, the interaction forces \vec{F}_k are taken to assert hard-disk behavior, i.e., to ensure that particles of diameter σ never overlap, and do not experience direct interaction forces else. The Brownian motion is driven by independent Wiener processes $d\vec{W}_k$ and dW_{φ_k} , where D_t and D_r are the respective diffusion coefficients. The particle mobility μ is chosen to obey the equilibrium detailed-balance condition, $\mu = \beta D_t$, where $\beta = 1/kT$ is the inverse temperature. Active motion is modeled as a fixed self-propulsion of velocity v_0 along the orientation vector of each particle, $\vec{n}(\varphi_k) = \vec{n}_k = (\cos \varphi_k, \sin \varphi_k)^T$. This term is formally treated as an (arbitrarily strong) non-equilibrium perturbation to the passive equilibrium dynamics.

We fix the units of length and time via the particle diameter σ and the translational diffusion time σ^2/D_t . This leaves two fundamental parameters to characterize the ABP motion, viz., the rotational diffusion coefficient D_r and the self-propulsion velocity v_0 .

The central quantity of ABP-MCT are the angle-resolved density fluctuations, $\varrho_l(\vec{q}) = \sum_{k=1}^N \exp[i\vec{q} \cdot \vec{r}_k] \exp[i l \varphi_k] / \sqrt{N}$, and the corresponding transient dynamical correlation functions

$$\Phi_{ll'}(\vec{q}, t) = \langle \varrho_l^*(\vec{q}) \exp[\Omega^\dagger t] \varrho_{l'}(\vec{q}) \rangle. \quad (2)$$

Here, angular brackets $\langle \cdot \rangle$ denote the usual *equilibrium* ensemble average, corresponding to the passive system. Such transient correlation functions are at the heart of the integration-through transients (ITT) formalism to derive expressions for non-equilibrium transport coefficients that are of generalized Green-Kubo type. In principle, they are accessible in experiment and simulation when the non-equilibrium perturbation – the particles' activity in our case – is suddenly switched on starting from a passive-equilibrium state.

The Smoluchowski operator Ω^\dagger that drives the time evolution is taken to correspond to the full non-equilibrium active dynamics. Translating the equations of motion, Eqs. (1), according to the theory of Markov processes one has

$$\Omega^\dagger = \sum_{k=1}^N D_t (\vec{\nabla}_k + \beta \vec{F}_k) \cdot \vec{\nabla}_k + D_r \partial_{\varphi_k}^2 + v_0 \vec{n}_k \cdot \vec{\nabla}_k. \quad (3)$$

The Smoluchowski operator is the sum of an equilibrium operator and an active driving term, $\Omega^\dagger = \Omega_0^\dagger + \delta\Omega^\dagger$, with $\delta\Omega^\dagger = v_0 \sum_k \vec{n}_k \cdot \vec{\nabla}_k$. Where convenient, we split off the rotational part of the operator, $\Omega_R^\dagger = D_r \sum_k \partial_{\varphi_k}^2$, denoting the remainder as its translational part, $\Omega_T^\dagger = \Omega^\dagger - \Omega_R^\dagger$.

A Mori-Zwanzig projection operator scheme allows to derive an exact equation of motion of the transient density correlation function [2], by projecting the dynamics onto the angle-resolved density fluctuations. One gets, in matrix notation with respect to the angular-mode indices,

$$\begin{aligned} \partial_t \Phi(\vec{q}, t) + \omega(\vec{q}) \cdot \mathbf{S}^{-1}(q) \cdot \Phi(\vec{q}, t) \\ + \int_0^t dt' \mathbf{m}(\vec{q}, t - t') \cdot (\mathbf{1} \partial_{t'} + \omega_R) \cdot \Phi(\vec{q}, t') = \mathbf{0}, \end{aligned} \quad (4)$$

to be solved with initial condition $\Phi(\vec{q}, 0) = \mathbf{S}(q)$. Here $S_{ll'}(q) = \delta_{ll'} S_l(q)$ is the equilibrium static structure factor of the passive system, assumed to be a known input quantity to the theory. Since we assume the interaction potential between the particles to be spherically symmetric, the only non-trivial term is $S_0(q) \equiv S(q)$, while $S_l(q) = 1$ for all $l \neq 0$. In general, we will assume the system to remain homogeneous and isotropic, so that the positional ($l = l' = 0$) correlation functions depend on the wave vector \vec{q} only through its magnitude $q = |\vec{q}|$.

The matrix $\omega(\vec{q}) = \omega_T(\vec{q}) + \omega_R = -\langle \varrho_l^*(\vec{q}) \Omega^\dagger \varrho_{l'}(\vec{q}) \rangle$ is the (negative) matrix element of the Smoluchowski operator, separated into its contributions to the translational and the rotational degrees of freedom,

$$\omega_{T, ll'}(\vec{q}) = \delta_{ll'} q^2 D_t - \delta_{|l-l'|, 1} \frac{i q v_0}{2} e^{-i(l-l')\theta_q} S_l(q), \quad (5a)$$

$$\omega_{R, ll'} = \delta_{ll'} l^2 D_r. \quad (5b)$$

Here, $\vec{q} = q(\cos \theta_q, \sin \theta_q)$. The non-trivial properties of the solutions of Eq. (4) for active particles (as compared to the established solutions for passive particles) stem from the fact that $\omega_T(\vec{q})$ is a tri-diagonal matrix and couples different l -modes.

The memory kernel $\mathbf{m}(\vec{q}, t) = \mathbf{M}(\vec{q}, t) \cdot \omega_T^{-1}(\vec{q})$ is the focus of MCT approximations. Assuming that the major contribution to these retarded friction effects on the motion of particles stems from the overlap of fluctuating

forces with density-pair modes, MCT sets

$$M_{l_1 l_2}(\vec{q}, t) \approx \frac{n}{2} \frac{1}{(2\pi)^2} \int d\vec{k} \sum_{l_3 l_4 l_3' l_4'} \mathcal{V}_{l_1 l_3 l_4}^\dagger(\vec{q}, \vec{k}, \vec{p}) \times \Phi_{l_3 l_3'}(\vec{k}, t) \Phi_{l_4 l_4'}(\vec{p}, t) \mathcal{V}_{l_2 l_3' l_4'}(\vec{q}, \vec{k}, \vec{p}) \quad (6)$$

with $n = N/V$ the density of the system, $\vec{q} = \vec{k} + \vec{p}$, and vertices $\mathcal{V}^\dagger = \mathcal{V} + \delta\mathcal{V}^\dagger$. The vertex \mathcal{V} is the same as in the passive-equilibrium theory,

$$\mathcal{V}_{l_1 l_3 l_4}(\vec{q}, \vec{k}, \vec{p}) = D_t \delta_{l_1, l_3 + l_4} \left[(\vec{q} \cdot \vec{k}) c_{l_3}(k) + (\vec{q} \cdot \vec{p}) c_{l_4}(p) \right], \quad (7a)$$

while the active contribution enters only \mathcal{V}^\dagger ,

$$\delta\mathcal{V}_{l_1 l_3 l_4}^\dagger(\vec{q}, \vec{k}, \vec{p}) = \frac{i v_0}{2} \delta_{|l_1 - l_3 - l_4|, 1} S_{l_1}(q) \times \left[k e^{-i(l_1 - l_3 - l_4)\theta_k} S_{l_1 - l_4}(k) (c_{l_1 - l_4}(k) - c_{l_3}(k)) + p e^{-i(l_1 - l_3 - l_4)\theta_p} S_{l_1 - l_3}(p) (c_{l_1 - l_3}(p) - c_{l_4}(p)) \right]. \quad (7b)$$

In these expressions, $c_l(q)$ is the direct correlation function, related to the static structure factor by $S_l(q) = (1 - n c_l(q))^{-1}$. In particular, $c_l(q) = 0$ for all $l \neq 0$.

B. Mode-Coupling Theory for Tagged-Particle Motion

We now consider a tagged (tracer) particle embedded in the N -particle system described above, with position \vec{r}_s and orientation φ_s . Its equation of motion shall be as Eq. (1), where the three relevant parameters are the diffusion coefficients D_t^s and D_r^s , and the tagged-particle self-propulsion velocity v_0^s . The interaction forces between the tracer and the host-system particles can in principle also differ from the one among the host particles; for example, the tracer could be of different size. For simplicity, we will not consider this in the present contribution, but we will specifically allow for the case of a passive tracer in an active bath, or vice versa, i.e., we will consider the case $v_0^s \neq v_0$.

The tagged-particle density fluctuations $\varrho_i^s(\vec{q}) = \exp[i\vec{q} \cdot \vec{r}_s] \exp[i l \varphi_s]$ define the tagged-particle transient density correlation function

$$\phi_{ll'}^s(\vec{q}, t) = \langle \varrho_l^{s*}(\vec{q}) \exp[\Omega^\dagger t] \varrho_{l'}^s(\vec{q}) \rangle, \quad (8)$$

where Ω^\dagger is given by Eq. (3) with the sum over particles extended to include the tagged particle. The derivation of the MCT equations of motion for $\phi^s(\vec{q}, t)$ proceeds in analogy to the derivation for the collective counter-part $\Phi(\vec{q}, t)$:

A Mori-Zwanzig projection onto the tagged-particle density fluctuations, using the projection operator $\mathcal{P} =$

$\sum_l \varrho^s(\vec{q}) \langle \varrho_l^{s*}(\vec{q})$ together with the Dyson decomposition

$$\partial_t \exp[\Omega^\dagger t] = \Omega^\dagger \mathcal{P} \exp[\Omega^\dagger t] + \Omega^\dagger \mathcal{Q} \exp[\Omega^\dagger \mathcal{Q} t] + \Omega^\dagger \mathcal{Q} \int_0^t dt' \exp[\Omega^\dagger \mathcal{Q}(t-t')] \Omega^\dagger \mathcal{P} \exp[\Omega^\dagger t'], \quad (9)$$

yields an equation of motion for the density-correlation function: inserting Eq. (9) into Eq. (8),

$$\partial_t \phi^s(\vec{q}, t) = -\omega^s(\vec{q}) \cdot \phi^s(\vec{q}, t) + \int_0^t dt' \mathbf{K}^s(\vec{q}, t-t') \cdot \phi^s(\vec{q}, t') \quad (10)$$

where $\omega^s(\vec{q})$ is given by the analog of Eq. (5),

$$\omega_{T, ll'}^s(\vec{q}) = \delta_{ll'} q^2 D_t^s - \delta_{|l-l'|, 1} \frac{i q v_0^s}{2} e^{-i(l-l')\theta_q}, \quad (11)$$

and $\omega_{R, ll'}^s = \delta_{ll'} l^2 D_r^s$. The Mori-Zwanzig memory kernel is given by

$$\mathbf{K}_{ll'}^s(\vec{q}, t) = \left\langle \varrho_l^s(\vec{q})^* \Omega^\dagger \mathcal{Q} \exp[\Omega^\dagger \mathcal{Q} t] \Omega^\dagger \varrho_{l'}^s(\vec{q}) \right\rangle. \quad (12)$$

In this expression, the spherical symmetry of the direct particle interactions imposes $\Omega_R^\dagger \varrho_{l'}^s(\vec{q}) \in \text{span}_m \{ \varrho_m^s(\vec{q}) \}$, and together with the fact that Ω_R^\dagger is self-adjoint with respect to the scalar product defined by the equilibrium average, it implies that to both sides of the exponential in Eq. (12), one can replace Ω^\dagger by Ω_T^\dagger .

Equation (10) is treated further in order to rewrite the memory kernel $\mathbf{K}^s(\vec{q}, t)$ into a friction memory kernel: we set $\mathcal{P}' = -\sum_{ll'} \varrho_l^s(\vec{q}) \langle \omega_{ll'}^s \rangle^{-1} \langle \varrho_{l'}^{s*}(\vec{q}) \Omega_T^\dagger$ to take out the one-particle reducible dynamics by a further Dyson decomposition,

$$\exp[\Omega^\dagger \mathcal{Q} t] = \exp[\Omega^\dagger \mathcal{Q}' \mathcal{Q} t] + \int_0^t dt' \exp[\Omega^\dagger \mathcal{Q}(t-t')] \Omega_T^\dagger \mathcal{P}' \mathcal{Q} \exp[\Omega^\dagger \mathcal{Q}' \mathcal{Q} t']. \quad (13)$$

Inserting into Eq. (12) results in

$$\mathbf{K}^s(t) = \mathbf{M}^s(t) - \int_0^t dt' \mathbf{K}^s(t-t') \cdot \omega_T^{s,-1} \cdot \mathbf{M}^s(t') \quad (14)$$

(dropping the \vec{q} dependence for notational convenience). Equations (10) and (14) can be combined to a single equation of motion for the density correlator,

$$\partial_t \phi^s(\vec{q}, t) + \omega^s(\vec{q}) \cdot \phi^s(\vec{q}, t) + \int_0^t dt' \mathbf{m}^s(\vec{q}, t-t') \cdot (\mathbf{1} \partial_{t'} + \omega_R^s) \cdot \phi^s(\vec{q}, t') = \mathbf{0}, \quad (15)$$

where we have set $\mathbf{m}^s(t) = \mathbf{M}^s(t) \cdot \omega_T^{s,-1}$. The exact microscopic expression for the irreducible memory kernel

is as in Eq. (12), with the replacement of the projected time-evolution operator by the further reduced one,

$$M_{ll'}^s(\vec{q}, t) = \left\langle \varrho_l^s(\vec{q}) \Omega_T^\dagger \mathcal{Q} \exp[\mathcal{Q} \Omega^\dagger \mathcal{Q}' \mathcal{Q} t] \mathcal{Q} \Omega_T^\dagger \varrho_{l'}^s(\vec{q}) \right\rangle. \quad (16)$$

MCT proceeds by approximating this memory kernel in terms of density pair modes. For the description of tagged-particle motion, the first non-trivial overlap is with the mixed modes $\varrho_{l_3}^s(\vec{k}) \varrho_{l_4}^s(\vec{p})$, so that inserting a projector onto such pairs to both sides of the exponential operator in Eq. (16), and splitting the resulting dynamical four-point correlation function into a product of two-point correlation functions, one obtains

$$M_{l_1 l_2}^s(\vec{q}, t) \approx \frac{n}{(2\pi)^2} \int d\vec{k} \sum_{l_3 l_4} \mathcal{W}_{l_1 l_3 l_4}^s(\vec{q}, \vec{k}) \times \Phi_{l_3, 0}(\vec{k}, t) \phi_{l_4 l_2}^s(\vec{p}, t). \quad (17)$$

In this expression, we have already made use of the fact, that the equilibrium part of the vertex is obtained in analogy to Eq. (7a), but due to the assumption of a tagged particle that is separate from the N host particles, a further symmetry under $\vec{k} \leftrightarrow \vec{p}$ allows to reduce the integral to twice that over the first term in the vertex expression. Making further use of the symmetry of the interaction potential, which ensures that all $c_l(q)$ with $l \neq 0$ vanish, the tagged-particle vertex can be summarized as

$$\mathcal{W}_{l_1 l_3 l_4}^s(\vec{q}, \vec{k}) = (D_t^s c^s(k))^2 \left[\delta_{l_1 l_4} \delta_{l_3 0} (\vec{q} \cdot \vec{k})^2 + \delta_{|l_1 - l_3 - l_4|, 1} \frac{i(\vec{q} \cdot \vec{k}) k e^{-i(l_1 - l_3 - l_4)\theta_k}}{2D_t^s} (v_0 S(k) \delta_{l_1 l_4} - v_0^s \delta_{l_3 0}) \right] \quad (18)$$

The tagged-particle direct correlation function $c^s(k)$ quantifies the interactions between the tracer particle and the host-system particles. In the simplest case of a structurally identical (but possibly different in activity) tracer, $c^s(k) = c(k)$.

In summary, the tagged-particle correlation functions are determined from a MCT memory equation with a memory kernel $\mathbf{M}^s(\vec{q}, t)$ that couples bi-linearly to the collective density correlators $\Phi(\vec{k}, t)$, and the tagged-particle correlators $\phi^s(\vec{p}, t)$. Thus, the equations can be solved once the collective dynamics has been determined.

C. Small-Wavenumber Limit

The positional tagged-particle correlation function is connected to the MSD of the tracer particle in the low- q limit,

$$\phi_{00}^s(q, t) = 1 - \frac{q^2}{4} \delta r^2(t) + \mathcal{O}(q^4) \quad (19)$$

in two spatial dimensions. It is thus instructive to discuss the $q \rightarrow 0$ limit of the MCT memory kernel $\mathbf{m}^s(\vec{q}, t)$. We

include this discussion here for completeness, although a detailed discussion of the MSD is outside the scope of the present contribution and is relegated to a separate publication [5].

The discussion is simplified by noting the transformation rule for the correlation functions under a rotation of \vec{q} . Invariance of the equilibrium distribution and the Smoluchowski operator under a rotation of the coordinate system implies $\Phi(\vec{q}', t) = \mathbf{u}^\dagger(\psi) \cdot \Phi(\vec{q}, t) \cdot \mathbf{u}(\psi)$ if \vec{q}' is obtained from rotating \vec{q} by an angle ψ and $u_{ll'}(\psi) = \delta_{ll'} \exp[i l \psi]$ is the unitary representation of the rotation group. The quantities

$$\tilde{\Phi}_{ll'}(q, t) = e^{i(l-l')\theta_q} \Phi_{ll'}(\vec{q}, t) \quad (20)$$

are thus functions of the wave vector through $q = |\vec{q}|$ only. We define corresponding isotropized matrices for the other quantities that appear in the equations of motion and denote them by tildes. It is readily checked that the Mori-Zwanzig equations of motion are invariant under this mapping.

There further holds $\tilde{\Phi}_{-l, -l'}^s(\vec{q}, t) = (-)^{l-l'} \tilde{\Phi}_{ll'}(\vec{q}, t)$, and it follows that the diagonal elements are isotropic and even functions of q . In particular, $\tilde{\Phi}_{00}(q, t)$ is indeed isotropic and real-valued in agreement with Eq. (19).

Since $\tilde{\mathbf{m}}^s(q, t) = \tilde{\mathbf{M}}^s(q, t) \cdot \tilde{\omega}_T^{s,-1}(q)$, the discussion of the low- q limit requires an expression for the inverse of $\tilde{\omega}_T^s(q)$. Note that the latter is a symmetric tri-diagonal matrix,

$$\tilde{\omega}_{T, ll'}^s(q) = \delta_{ll'} D_t^s q^2 - \delta_{|l-l'|, 1} \frac{i q v_0^s}{2}. \quad (21)$$

This simple structure allows to derive a closed form for the matrix elements of its inverse,

$$(\tilde{\omega}_T^s)_{ll'}^{-1} = \frac{1}{\Delta} \left(\frac{i q v_0^s}{D_t^s q^2 + \Delta} \right)^{|l-l'|} \quad (22)$$

setting $\Delta = \sqrt{(D_t^s q^2)^2 + (v_0^s q)^2}$. This is readily checked by direct computation of $\tilde{\omega}_T^s \cdot \tilde{\omega}_T^{s,-1}$. A direct derivation of this result is given in Appendix A.

It is worth stressing that implicit in this result is the recognition that the Mori-Zwanzig equations based on the angle-resolved density fluctuations are formulated for elements $\phi_{ll'}^s(\vec{q}, t)$ of an infinite-dimensional matrix algebra spanned by the angular indices. It is customary (and necessary for numerical computation) to introduce some angular-index cutoff L such that $l, l' \in [-L, L]$. However, the operations of introducing such cutoff and of taking the inverse in the limit $q \rightarrow 0$ do not commute for $\tilde{\omega}_T^s(q)$. Numerical evaluation in fact confirms that for $v_0^s \neq 0$, the inversion of the finite-dimensional matrix yields an asymptotic behavior $\sim 1/q^2$ for the (00) element of the inverse for all even cutoff values L , while the same element approaches a constant for all L odd. On the infinite-dimensional algebra, Eq. (22) confirms the asymptote $1/(v_0^s q)$ for $l = l' = 0$ and $v_0^s \neq 0$. Obtaining

this asymptote is crucial in deriving the correct $q \rightarrow 0$ limit of the ABP-MCT equations.

It is also remarkable that the $q \rightarrow 0$ limit of Eq. (22) does not commute with $v_0^s \rightarrow 0$. In physical terms, any small tracer activity is eventually felt at large enough length scales, i.e., if $q \ll q_* = v_0^s/D_t^s$. Expansion of Eq. (22) yields

$$(\tilde{\omega}_T^s)_{ll'}^{-1} \sim \begin{cases} 1/(D_t^s q^2) \delta_{ll'} & \text{for } v_0^s = 0, \\ \frac{1}{v_0^s q} i^{|l-l'|} \left(1 - |l-l'| \frac{q}{q_*}\right) + \mathcal{O}(q) & \text{for } v_0^s \neq 0. \end{cases} \quad (23)$$

It requires some care to check that the $q \rightarrow 0$ expansion of the memory integral in Eq. (15) remains regular and produces terms of leading order $\mathcal{O}(q^2)$ in the case of the (00) element, as required by Eq. (19). In the equilibrium theory, this is readily noted by realizing that the vertex \mathcal{W}^s , Eq. (18) is of $\mathcal{O}(q^2)$, so that $\tilde{m}_{00}^s(q, t) \sim \mathcal{O}(q^0)$ combines with the $\mathcal{O}(q^2)$ order of $\partial_{t'} \phi_{00}^s(q, t)$. The appearance of non-diagonal terms in both $\tilde{\mathbf{m}}^s(q, t)$ and $\tilde{\phi}^s(q, t)$, and of a potentially ‘‘dangerous’’ term of $\mathcal{O}(q)$ in the vertex \mathcal{W}^s , complicate matters in the ABP-MCT. After checking the different contributions individually, as detailed in Appendix B, one obtains an equation for the MSD,

$$\begin{aligned} \partial_t \delta r^2(t) + \int_0^t dt' \hat{m}_{00}^s(t-t') \partial_{t'} \delta r^2(t') \\ = 4D_t^s - 2iv_0^s \sum_{\pm} \hat{\phi}_{\pm 1,0}^s(t) \\ + 4 \sum_{\pm} \int_0^t dt' \hat{m}_{0,\pm 1}^s(t-t') (\partial_{t'} + D_r^s) \hat{\phi}_{\pm 1,0}^s(t'), \end{aligned} \quad (24)$$

where $\hat{m}_{ll'}(t) = \lim_{q \rightarrow 0} \tilde{m}_{ll'}(q, t)/q^{|l-l'|}$ for $|l-l'| \leq 1$ Equation (24) reduces to the well known MCT equation for the MSD of a passive tracer when $v_0^s = 0$, where the non-diagonal elements of the correlators vanish. In the case of an active tracer particle, a further equation determines the off-diagonal low- q correlator, $\hat{\phi}_{\pm 1,0}^s(t) = \lim_{q \rightarrow 0} \tilde{\phi}_{\pm 1,0}^s(q, t)/q$,

$$\begin{aligned} (\partial_t + D_r) \hat{\phi}_{\pm 1,0}^s(t) = \frac{iv_0^s}{2} \\ - 2 \int_0^t dt' \hat{m}_{\pm 1, \pm 1}^s(t-t') (\partial_{t'} + D_r) \hat{\phi}_{\pm 1,0}^s(t'). \end{aligned} \quad (25)$$

Explicit expressions for the memory kernels are given in Appendix B.

The equations (24) and (25) determine the MSD of an active or passive tracer in an active or passive bath, once the corresponding tagged-particle correlation functions at finite \bar{q} have been determined and with these the low- q memory kernels $\hat{\mathbf{m}}(t)$.

D. Numerical Solution of MCT Equations

The MCT equations were solved numerically with an algorithm outlined in Ref. [2], using a discrete wave-number grid $q_i = (i+1)\Delta q/2$, $i = 1, \dots, M$ with a grid size of $M = 128$ and step size $\Delta q \simeq 0.3$, implying a large-wave-number cutoff $Q = 40\sigma$. The integrals are performed for \bar{q} placed along the y -axis, and the correlation functions for different wave-vector orientations that are required in the memory-kernel integrals are obtained by their known transformation behavior under spatial rotations [2]. Angular-mode indices were considered with a cutoff $l \in [-L, L]$ with $L = 1$, which is deemed sufficient for the range of self-propulsion velocities that we study within the theory here.

The equilibrium static structure factor was obtained from density-functional theory (DFT) for two-dimensional hard disks [6]. This differs slightly from the structure factor used in previous studies of two-dimensional hard disks in MCT, where either modified hypernetted-chain (MHNC) has been used [7] or the empirical Baus-Colot formula [2]. No qualitative changes are imposed by these different choices; only the predicted glass-transition point depends both on the choice of $S(k)$ and the parameters of the discretization in the wave-vector integrals.

E. Brownian Dynamics Simulations

To compare the theoretical predictions with simulation results, we performed ED-BD simulations of size-polydisperse hard-disk systems with $N = 1000$ particles (adjusting the box size to achieve the desired packing fraction for any given realization of polydispersity). Particle sizes were drawn randomly from a uniform distribution of width 0.1.

The ED-BD algorithm has been described in detail for passive systems [4]. For every Brownian time step of length τ_B , the particles are assigned random Gaussian displacements Δx with a variance that sets the short-time diffusion coefficient. To resolve particle overlaps, the displacements are translated into pseudo-velocities, $v = \Delta x/\tau_B$, and an event-driven molecular-dynamics simulation segment of length τ_B is performed with elastic collisions between the particles. This algorithm reproduces the Smoluchowski dynamics of the passive system if τ_B is chosen not too large [4].

The algorithm is extended ad hoc to active particles by assigning Gaussian displacements to the particles with an individual drift corresponding to the active driving term. For this, also particle orientation angles are tracked and incremented by Gaussian displacements to establish rotational diffusion. A version of this algorithm has first been used by Ni et al. [1] for studying the high-density dynamics of ABP.

For each density we performed at least 200 runs to accumulate statistics for the dynamical correlation func-

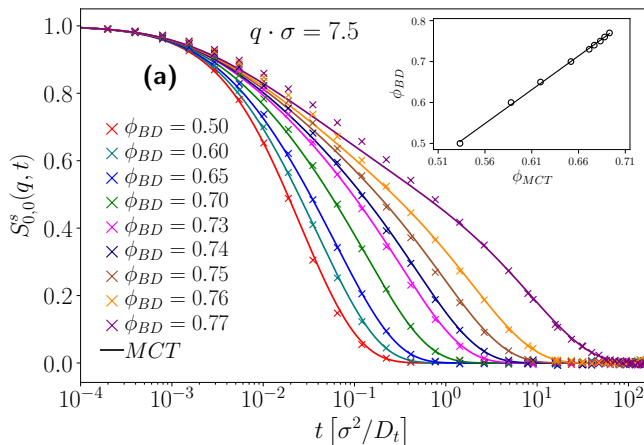


FIG. 1. Tagged-particle density correlation function $S_{0,0}^s(q, t)$ for passive hard-disk systems of packing fraction ϕ_{BD} as indicated, at wave number $q\sigma = 7.5$. Symbols are results from Brownian dynamics computer simulations, lines are MCT results for packing fractions ϕ_{MCT} adjusted to give the best description of the data (see inset for the linear relation between ϕ_{BD} and ϕ_{MCT}).

tions. The systems were equilibrated first, and then the self-propulsion term was switched on and the systems were brought into stationary state by preparation runs of at least 10^4 Brownian time steps. To study the tracer dynamics, an individual particle was selected within each simulated configuration to closely match the average size of the particles (in order to avoid size-disparity effects that become visible when averaging the motion of tracers of different sizes in the different simulation runs). To improve the statistics, correlation functions were averaged over different starting points in the stationary simulations. For the fully active system, the simulation statistics was also sufficient to calculate the transient dynamical correlation functions obtained from the simulation-ensemble average over the passive-equilibrium starting configurations.

III. RESULTS

A. Passive Dynamics

We begin by establishing the level of accuracy that can be expected from MCT by comparing to our simulations of a passive hard-disk system. It is well known that MCT provides a semi-quantitative description of the relaxation dynamics in a density range just below the glass-transition density, after an adjustment of packing fractions [8]

With such an adjustment of the packing fraction, our solutions of the MCT equations for passive hard disks indeed match the computer simulation results very well. Anticipating that the glassy dynamics is driven by fluctuations around the nearest-neighbor peak in the static

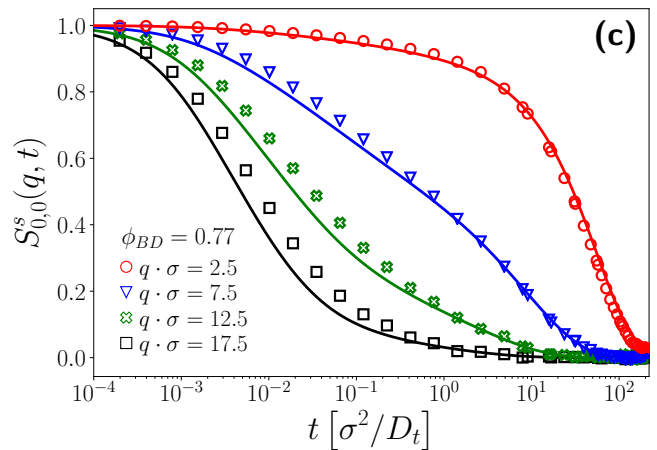


FIG. 2. Tagged-particle density correlation function $S_{0,0}^s(q, t)$ for passive hard-disk systems of packing fraction $\phi_{BD} = 0.77$, for different wave numbers as indicated. Symbols are BD simulation results, lines are MCT with effective packing fractions.

structure factor, the adjustment of ϕ_{MCT} is performed at $q\sigma = 7.5$. Due to its better sampling statistics, we chose to fit the tagged-particle density correlation function rather than its collective counterpart; at this wave number, no essential change is expected from this [8]. In agreement with earlier studies of similar spirit [7, 8] the thus adjusted MCT gives a quantitative account of the dynamics (Fig. 1). Moreover, a free fit of ϕ_{MCT} for a range of simulations at $\phi_{BD} \geq 0.5$ yields an almost perfectly linear relationship between the two quantities (inset of Fig. 1). Considering that within MCT asymptotically close to the glass transition, a distance parameter that is asymptotically linearly related to the control-parameter distance governs the long-time dynamics, the linear relationship found from the free fit corroborates that the adjustment procedure accounts for a well-understood error of MCT in predicting quantitatively the numerical value of the glass-transition point.

Once the mapping of packing fractions is established for the density-fluctuation dynamics of the relevant length scale, MCT also accounts well for the dynamics at other wave numbers in the range covering the relevant variations in $S(q)$ (Fig. 2). The agreement remains very good down to $q\sigma \approx 2.5$ in our simulations, although it is known from similar comparisons in three-dimensional hard-sphere-like systems that for still smaller q , deviations systematically set in [8]. Also as found previously in 3D, the description of the short-time dynamics deteriorates at large q . These effects appear similarly in our 2D comparison and establish the relevant q range over which MCT is expected to quantitatively account for the dynamics.

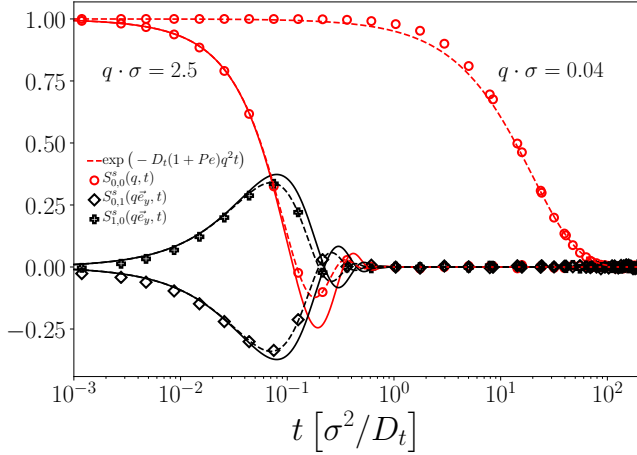


FIG. 3. Correlation functions $S_{l,l'}^s(\vec{q}, t)$ for a single active Brownian particle with self-propulsion velocity $v_0^s = 8 D_t/\sigma$ and rotational diffusion coefficient $D_r = 1 D_t/\sigma^2$, at a wave vector $\vec{q} \cdot \sigma = 2.5\vec{e}_y$ and $0.04\vec{e}_y$ (as labeled). Symbols are BD simulation results. Solid lines are the solution of the Mori-Zwanzig equations with angular-mode cutoff $L = 1$, dashed lines with $L = 10$.

B. Low-Density Active Dynamics

The density correlation functions of a single ABP have been discussed analytically by Kurzthaler et al. [9]. They proceeded by an expansion of the characteristic function in terms of suitable eigenfunctions of the single-particle Smoluchowski operator, the Mathieu functions. The calculation is readily extended to the correlation functions for $(ll') \neq (00)$.

Since the Mori-Zwanzig equation without a memory kernel is an exact rewriting of the equation of motion, it necessarily needs to coincide with this analytical result, although the equivalence is somewhat tedious to show [10]. It is nevertheless worth checking the quality of the Mori-Zwanzig solution with a finite l -cutoff. For the range of parameters that are of interest here, indeed already a cutoff $L = 1$ gives good qualitative agreement (solid lines in Fig. 3), although larger L would be needed to increase the quantitative description of the oscillatory decay of the correlation function in a q -range that probes the length scales of persistent motion of the ABP.

C. Active Tracer in a Passive Suspension

A first test of the inclusion of self-propulsion forces in ABP-MCT is provided by the dynamics of a single ABP embedded in a dense host suspension of passive particles. The tracer dynamics decays faster with increasing self-propulsion velocity, v_0^s , of the tracer, although the overall influence of self-propulsion in the dense host suspension is relatively weak (Fig. 4). ABP-MCT somewhat underestimates this effect, but in particular at wave numbers q

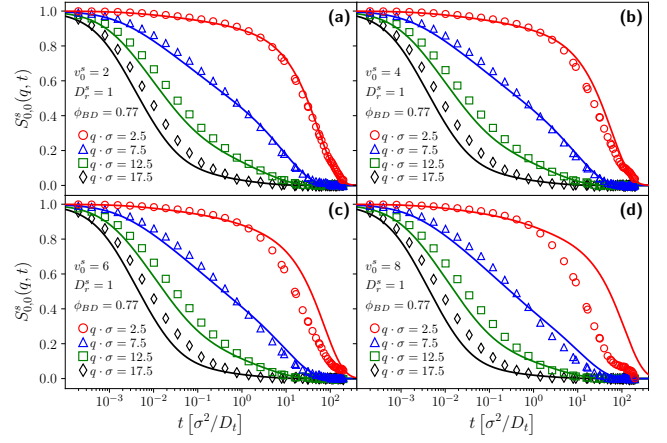


FIG. 4. Self-intermediate scattering function of an active tracer in a passive bath, BD simulations (open symbols) compared with MCT (lines), at different wave numbers as indicated and fixed packing fraction $\phi = 0.77$. (a)–(d) show different self-propulsion velocities of the tracer, v_0^s .

related to the structure-factor maximum, the theory is in good agreement with the simulation. Deviations become most pronounced for low q and large v_0^s ; the deviations at low q are in fact expected already on the basis of passive MCT [8].

The influence of the tracer-particle activity in a passive host medium is most pronounced at low q . This is highlighted by the q -dependent structural relaxation times extracted from the correlation functions, Fig. 5. Overall, ABP-MCT provides a good description of the simulation data, except for the highest density, $\phi = 0.77$, studied in the simulations in the case of $D_r^s = 1$. There, the theory predicts a crossing of the τ^s -vs- q curves for different v_0^s of which we find no evidence in the simulations. It has to be kept in mind, that generally, MCT does not accurately account for the relaxation dynamics very close to the glass transition, and the discrepancy observed for the low- q data at $\phi = 0.77$ may well be due to that.

Increasing the persistence length of active motion at the same self-propulsion speed and density is predicted by ABP-MCT to cause a stronger enhancement of relaxation; the simulations for $D_r^s = 1$ and $D_r^s = 0.05$ shown in Fig. 5 show this effect for the highest packing fraction and the lower range of v_0^s that we have studied here.

D. Passive Tracer in an Active Suspension

The passive tracer dynamics in a suspension of ABP provides an interesting test case for the application of microrheological techniques in active fluids. Qualitatively, the correlation functions display the same features as those discussed above for an active tracer in a passive bath (Fig. 6): with increasing activity, the relaxation time shortens, similarly for all wave numbers. The effect of an active bath on a passive tracer is, as perhaps

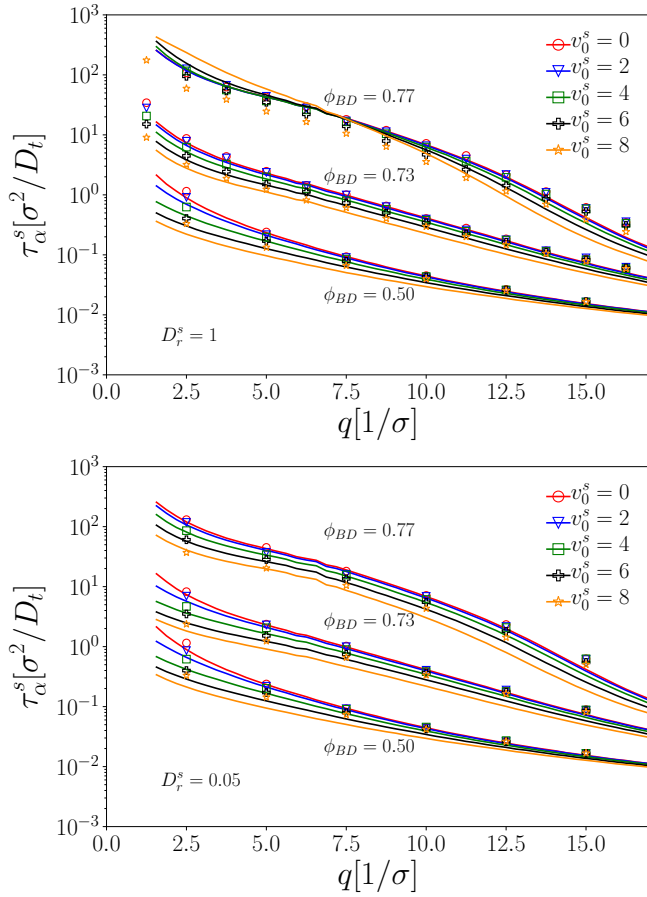


FIG. 5. Relaxation time of the SISF for different ϕ as indicated, active tracer in passive host system. Symbols are BD, lines are MCT. Top panel: $D_r^s = 1$, bottom panel $D_r^s = 0.05$.

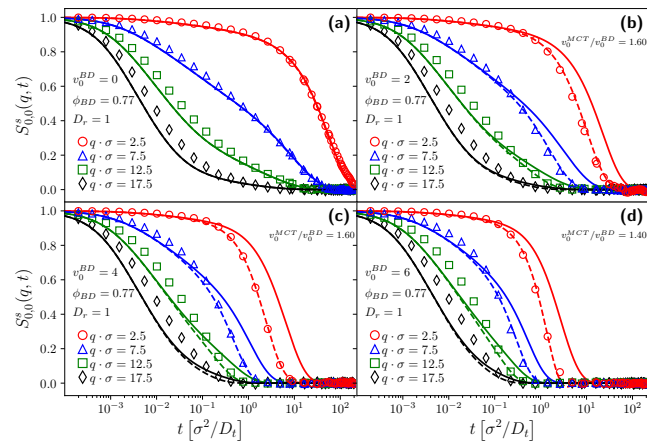


FIG. 6. SISF of passive tracer in active bath. Symbols are BD simulation results, full lines are from MCT. Dashed lines represent MCT with a further empirical mapping of self-propulsion velocities, $v_0^{\text{MCT}} \approx 1.5v_0^{\text{BD}}$ (as labeled).

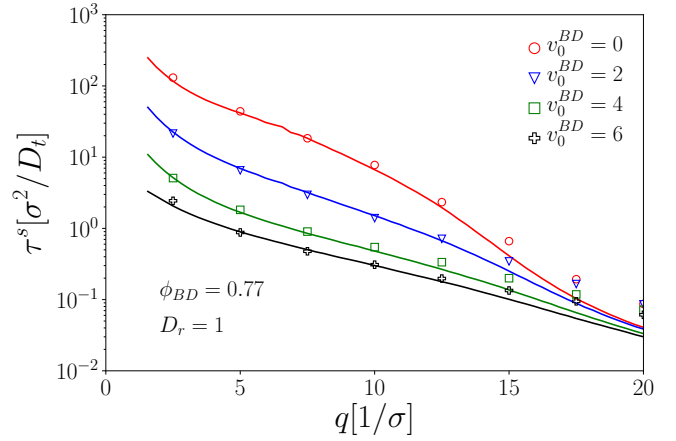


FIG. 7. Wave-number dependent structural relaxation times $\tau^s(q)$ of a passive tracer in an active host system, from BD (symbols) and MCT (lines), at a fixed packing fraction $\phi = 0.77$, and various self-propulsion speeds as labeled.

might be expected, much stronger than that of a single active tracer of the same self-propulsion velocity within a passive bath.

Again, MCT is in good qualitative agreement with our BD simulation results. However, MCT underestimates the effect of bath activity on the tracer, i.e., the predicted correlation functions decay too slowly.

It is also a known effect from other non-equilibrium extensions of MCT, that the theory's approximations tend to underestimate the tendency to fluidization. This is also in line with the general trend of MCT to overestimate glassiness. Already for sheared colloidal suspensions, an empirical strain scale was introduced, and it was found that after such adjustment, the results of MCT are again in good, even quantitative, agreement with observation. Motivated by this finding, we also compare our BD simulations with the MCT predictions where, in addition to the density mapping that is kept fixed throughout after adjusting it for the purely passive system, we also introduce an empirical velocity rescaling. The result (dashed lines in Fig. 6) shows that a roughly parameter-independent mapping of $v_0^{\text{MCT}} = 1.5v_0^{\text{BD}}$ is sufficient to bring MCT in semi-quantitative agreement with simulation.

The relaxation time $\tau^s(q)$ for the case of a passive tracer in the active bath (Fig. 7) demonstrates the much stronger influence of self-propulsion in this case. Here, the strong influence extends over the relevant q -range in structural relaxation, i.e., up to $q\sigma \approx 15$. One also notes that the hydrodynamic limit, where $\tau^s(q) \sim 1/q^2$, is reached only at $q\sigma \lesssim 2$, and there is an intermediate range of wave numbers where a weaker variation of τ^s with q becomes apparent. We shall return to this in the case of an active tracer in an active host system.

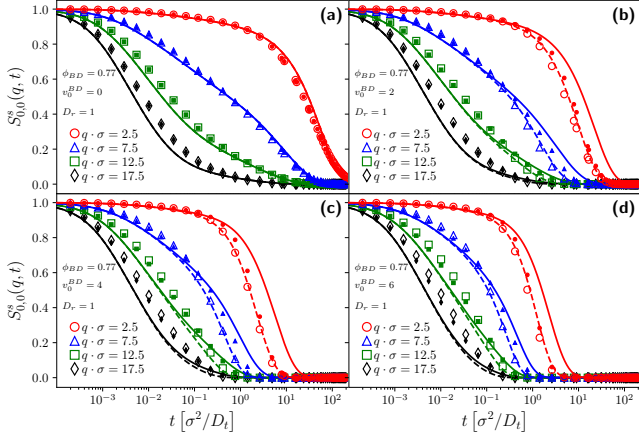


FIG. 8. Density correlation functions of an active tracer in an active bath; for fixed bath packing fraction $\phi_{BD} = 0.77$ and different self-propulsion velocities v_0^{BD} (panels (a)–(d)). Symbols as BD results, solid lines are MCT predictions for various wave numbers as indicated. Dashed lines show the result of MCT with an adjusted self-propulsion velocity $v_0^{MCT} = 1.5v_0^{BD}$.

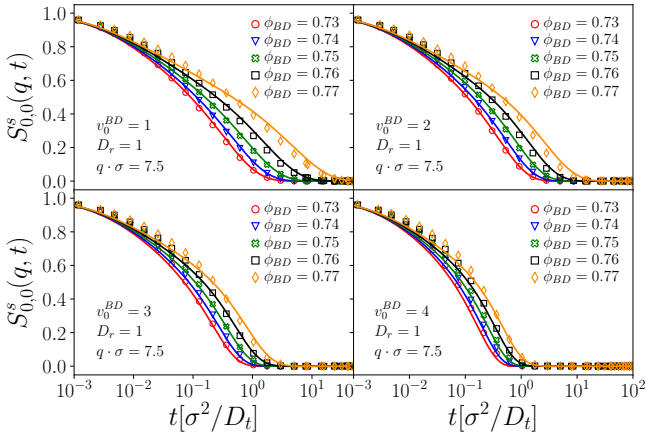


FIG. 9. SISF evolution active in active for different fixed v_0 , as a function of packing fraction ϕ .

E. Active Tracer in an Active Suspension

Finally, the dynamics of an active tracer particle in a fully active system displays qualitatively the similar features as the case of a passive tracer in the active bath that was just discussed. The density correlation functions at high densities still decay monotonically, and their relaxation time decreases with increasing v_0 (Fig. 8). As in the previous discussion, MCT qualitatively accounts for this enhanced relaxation, but it underestimates its effect. Again, this can be, for the range of self-propulsion velocities that we consider here, accounted for by a simple empirical adjustment $v_0^{MCT} = 1.5v_0^{BD}$, i.e., by assuming again that MCT underestimates the tendency of the nonequilibrium perturbation to fluidize the system.

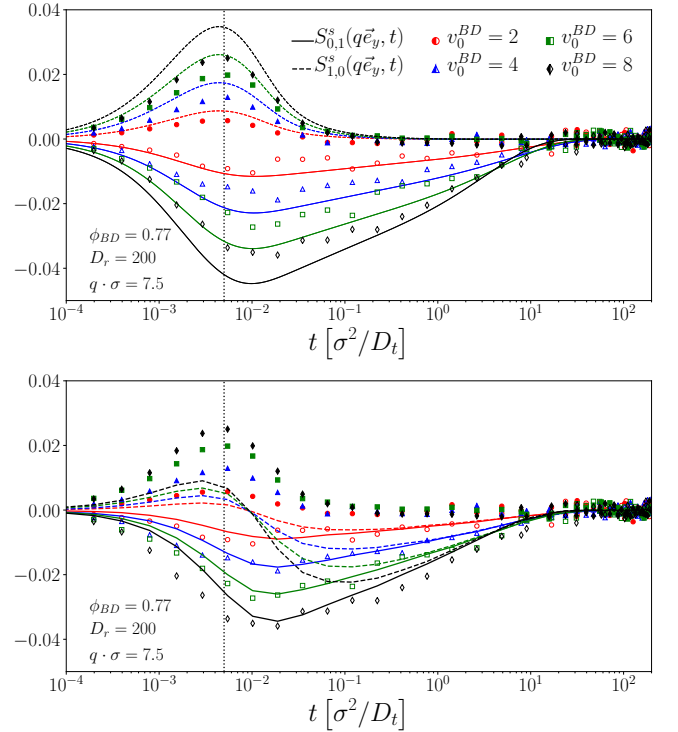


FIG. 10. Stationary and transient tagged-particle correlation functions $S_{l,l'}^s(\vec{q}, t)$ of the dense ABP system (packing fraction $\phi = 0.77$) with $D_r = 200 D_t / \sigma^2$, for $\vec{q}\sigma = x x \vec{e}_y$ and various self-propulsion velocities as indicated. TODO One panel compares transient BD with transient MCT for $(l, l') = (1, 0)$ (dashed/filled) and $(0, 1)$ (solid/open). One panel compares stationary BD with transient.

In Brownian dynamics that obey detailed balance, the backward Smoluchowski operator Ω^\dagger driving the time evolution is self-adjoint in the scalar product weighted with the corresponding equilibrium distribution function. The active-particle dynamics does not have the property of detailed balance, and hence Ω^\dagger is no longer self-adjoint.

In MCT, the resulting asymmetry extends to the long-time limits: one set of correlation functions decays on $1/D_r$, while the other does not. This striking prediction was interpreted as an effect of the transient nature of the correlation functions [2].

The BD simulations indeed confirm this (Fig. 10): to check the result, we consider simulations with $D_r = 200 D_t / \sigma^2$ such that $1/D_r$ is a time scale much shorter than the structural relaxation time of the system. Then, $S_{1,0}^s$ decays on $1/D_r$, while $S_{0,1}^s$ decays on τ . MCT qualitatively fits the results, although for larger v_0 , the quantitative agreement is slightly worse, as expected from the discussion above.

The BD simulations also allow to address the difference between the transient correlation functions considered in MCT, and the stationary correlation functions considered more commonly. Extracting both from BD simulations (Fig. 10), one notes that for times compara-

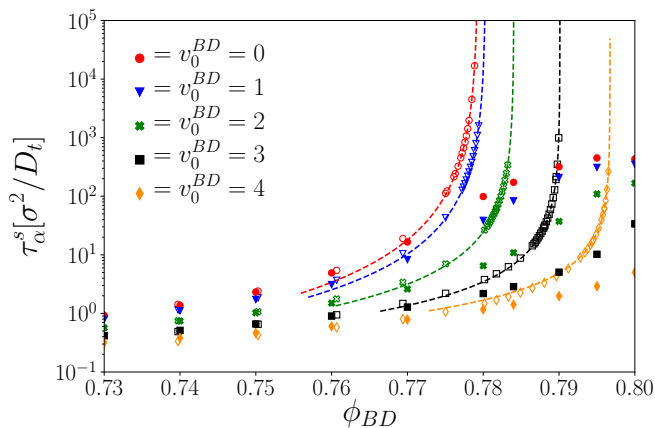


FIG. 11. Relaxation time τ as a function of ϕ , BD results (filled symbols) and MCT (open symbols) with corresponding power-law fits (dashed lines).

ble to $1/D_r$, the asymmetry remains, while for $t \gg 1/D_r$ the stationary correlation functions become symmetrical. This suggests, extending the MCT results bona fide, that also the nonergodicity parameters measured in the stationary ensemble will be symmetric.

In the high-density system, the tagged-particle dynamics of a tracer identical to the bath particles, and the collective dynamics at finite q are strongly coupled, and hence both can be taken as proxies to determine the structural relaxation time. Indeed, we confirm the expected power-law divergence within our MCT results for the tagged-particle dynamics (Fig. 11). The BD simulations qualitatively agree in a window of not too high packing fractions, with deviations becoming more pronounced for higher v_0 . At high densities, the MCT approximation neglects glass-like relaxation processes [12], and hence the BD simulation results deviate from the MCT power-law divergence.

The q -dependence of the relaxation times follows, in the regime of high densities and self-propulsion velocities covered here, the expected behavior known from passive systems (Fig. 12): as $q \rightarrow 0$, a divergence $\tau^s \sim 1/q^2$ is observed (dotted lines in the figure). But there opens a large intermediate regime, where the behavior is $\tau^s \sim 1/q$; note that from the free-particle dynamics and the inversion of the matrix $\omega^s(\vec{q})$ one indeed expects an $1/v_0^s q$ asymptote to govern the relaxation times.

There is a small difference in the relaxation times of the transient and the stationary correlation functions as obtained from simulation (open and filled symbols in Fig. 12).

IV. CONCLUSION

We have derived equations of motion for the angle-resolved tagged-particle density correlation functions of tracers in dense systems of active Brownian particles,

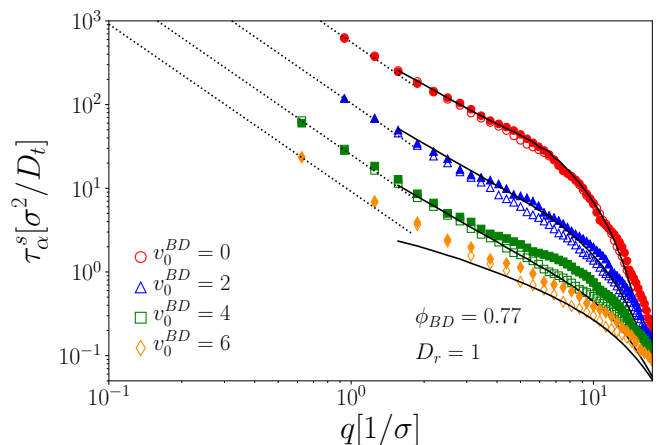


FIG. 12. q dependence of the relaxation time of the active tracer in the active bath; MCT results (lines) and BD simulation results (symbols; open: transient, filled: stationary), with $v_0^{\text{MCT}} = 1.5v_0^{\text{BD}}$ adjusted.

in the context of the mode-coupling theory of the glass transition and the integration-through transients framework. The numerical solutions of this ABP-MCT theory have been compared to computer simulations of hard-disk ABP for the different cases of active and passive tracers in active and passive host systems. Overall, we have found theory and simulation to be in good qualitative agreement, for a range of densities close to the glass transition, and for a range of self-propulsion speeds that is not too large. The theory, as known for the passive MCT, overestimates the slowness of structural relaxation, and hence the comparison to simulation data best proceeds with an empirical mapping of densities, and an empirical mapping of self-propulsion speeds in the case of an active host system. After such mapping, the agreement between theory and simulation is near-quantitative.

An interesting feature in the angle-resolved correlation functions is that they are in general non-symmetric matrices of the angular-mode indices. This reflects the non-equilibrium nature of the dynamics, and has first been noted in the ABP-MCT for the collective density fluctuations. We have confirmed this asymmetry directly in our Brownian dynamics (BD) simulations. The simulations point out an interesting difference in the transient correlation functions targeted by the ITT-MCT, and the stationary correlation functions more commonly accessed in experiment and simulation: while both remain asymmetric, there appears to be a time scale after which the time-evolution crosses over to a symmetric form of correlations (as perhaps more intuitively expected). The time scale is associated with the rotational persistence of the ABP; it is thus expected to also play an important role in determining, for example, signatures of persistent motion in other quantities such as the MSD (where superdiffusive regimes indicate the time windows of persistent swimming). Such investigation will be discussed elsewhere.

ACKNOWLEDGMENTS

We acknowledge funding from Deutsche Forschungsgemeinschaft (DFG), as part of the Special Priority Programme SPP 1726 ‘‘Microswimmers’’ (project Vo 1270/7).

Appendix A: Inversion of Frequency Matrix

A tridiagonal $n \times n$ matrix with elements a_{ij} such that $a_{ij} = 0$ whenever $|i-j| > 1$, can be inverted by employing a recursion formula for the elements α_{ij} of the inverse matrix. Setting $a_{ii} = b_i$, $a_{i,i+1} = c_i$, and $a_{i,i-1} = c_i$, Usmani [13] derives

$$\alpha_{ij} = \begin{cases} (-)^{i+j} c_i c_{i+1} \cdots c_{j-1} \theta_{i-1} \phi_{j+1} / \theta_n, & i < j, \\ \theta_{i-1} \phi_{i+1} / \theta_n, & i = j, \\ (-)^{i+j} a_{j+1} a_{j+2} \cdots a_i \theta_{j-1} \phi_{i+1} / \theta_n, & i > j, \end{cases} \quad (\text{A1})$$

where the sequences θ_i and ϕ_i are given by recursion relations,

$$\theta_i = b_i \theta_{i-1} - a_i c_{i-1} \theta_{i-2}, \quad \phi_i = b_i \phi_{i+1} - c_i a_{i+1} \phi_{i+2}, \quad (\text{A2})$$

with $\theta_0 = \phi_{n+1} = 1$ and $\theta_{-1} = \phi_{n+2} = 0$.

We apply this result for the $n \times n$ matrix ω_T^s given by Eq. (21) with cutoff L , setting $n = 2L + 1$, $i = l + L + 1$ and $j = l' + L + 1$ with $l, l' \in [-L, L]$. Identifying then $b_i = D_t q^2$, $a_i = c_i = -i v_0^s q / 2$, the recursion relations can be solved in closed form: setting $\Delta = \sqrt{(D_t q^2)^2 + (v_0^s q)^2}$, and $\beta_{\pm} = D_t q^2 \pm \Delta$, one obtains

$$\theta_i / \theta_n = \frac{2^{n-i} (\beta_+^{1+i} - \beta_-^{1+i})}{\beta_+^{1+n} - \beta_-^{1+n}}, \quad (\text{A3a})$$

$$\phi_i = \frac{(-)^{i+1-n}}{\Delta} \left[2^{i-2-n} (v_0^s q)^{2(n-i)} \left(\beta_+^{i-n} ((v_0^s q)^2 + 2D_t q^2 \beta_-) - \beta_-^{i-n} ((v_0^s q)^2 + 2D_t q^2 \beta_+) \right) \right] \quad (\text{A3b})$$

From this, the limit $L \rightarrow \infty$ at fixed l, l' and fixed q can be performed. Using $\lim_{L \rightarrow \infty} (\beta_- / \beta_+)^L = 0$, one finally gets Eq. (22).

Appendix B: Low- q Expansion of the Memory Kernel

The limit $q \rightarrow 0$ in the vertex, Eq. (18) is obtained noting $k = p - (\vec{q} \cdot \vec{p}) / p + \mathcal{O}(q^2/p)$ and $k \exp[\pm i \theta_k] = q \exp[\pm i \theta_q] - p \exp[\pm i \theta_p]$ for vectors $\vec{q} = \vec{k} + \vec{p}$. Note that the equilibrium contribution is already of $\mathcal{O}(q^2)$, so that in this case $\tilde{m}^s(q, t) = \mathcal{O}(q^0)$, and hence the (00) element of Eq. (15) is $\mathcal{O}(q^2)$ in leading order, compatible with the expression Eq. (19).

This is less obvious in the case of ABP. In particular, the low- q expansion of Eq. (18) contains terms of $\mathcal{O}(q)$. One needs to check that these potentially dangerous terms do not contribute in the Mori-Zwanzig equation. Inserting the small- q expansion of $\mathcal{W}^s(\vec{q}, \vec{k})$ into Eq. (17) and performing the integration over the angle θ_k in $\int d\vec{k} = \int k dk d\theta_k$, one obtains

$$\begin{aligned} \tilde{M}_{ll'}^s(q, t) &\sim \frac{n D_t^{s2}}{8\pi} \int dp \tilde{\phi}_{m'l'}^s(p, t) \times \\ &\left\{ q^2 p^3 (\delta_{l-l',-2} + \delta_{l-l',2} + 2\delta_{ll'}) c^s(p)^2 \tilde{\Phi}_{00}(p, t) \delta_{lm'} \right. \\ &\quad + \frac{i q p^3}{D_t^s} (\delta_{l-l',-1} + \delta_{l-l',1}) \tilde{w}_{l,mm'}(p) \tilde{\Phi}_{m0}(p, t) \\ &\quad - \frac{i q^2}{D_t^s} \delta_{ll'} \partial_p \left(p^3 \tilde{w}_{l,mm'}(p) \tilde{\Phi}_{m0}(p, t) \right) \\ &\quad \left. - \frac{i q^2 p^2}{D_t^s} (\delta_{l-l',-2} + \delta_{l-l',2}) \partial_p \left(p \tilde{w}_{l,mm'}(p) \tilde{\Phi}_{m0}(p, t) \right) \right\} \quad (\text{B1}) \end{aligned}$$

where we have defined

$$\tilde{w}_{l,mm'}(p) = (\delta_{|l-m'|,1} \delta_{m0} v_0^s - \delta_{lm'} \delta_{|m|,1} v_0 S(p)) c^s(p)^2. \quad (\text{B2})$$

For the passive tracer, $v_0^s = 0$, the term $\tilde{w}_{l,mm'}(p)$ is proportional to $\delta_{lm'}$, so that all terms appearing in the memory kernel, Eq. (B1), couple to $\tilde{\phi}_{ll'}^s(p, t)$. But since for this case, the matrix $\tilde{\omega}_T^s(q)$ remains diagonal, the Mori-Zwanzig equations that determine the off-diagonal elements of the correlation-function matrix decouple and, since $\tilde{\phi}_{ll'}^s(q, 0) = \delta_{ll'}$, these off-diagonal elements all identically vanish. The only contribution to $\tilde{m}_{ll'}^s(q, t)$ is thus from the diagonal elements, all of $\mathcal{O}(q^2)$ in leading order. One obtains the only memory kernel that enters the MSD equation, Eq. (24), for the passive tracer:

$$\begin{aligned} \hat{m}_{00}^s(t) &= \frac{n D_t^s}{4\pi} \int dp \tilde{\phi}_{00}^s(p, t) \left\{ p^3 c^s(p)^2 \tilde{\Phi}_{00}(p, t) \right. \\ &\quad \left. + \frac{i}{2 D_t^s} \delta_{|m|,1} \partial_p p^3 v_0 S(p) c^s(p)^2 \tilde{\Phi}_{m0}(p, t) \right\}. \quad (\text{B3}) \end{aligned}$$

The first term is the known contribution from passive MCT [7].

In the case of an active tracer particle, Eq. (B1) is simplified by noting a further symmetry of the correlation functions: inverting the coordinate system around the x -axis, $\{x_k, y_k, \varphi_k\} \mapsto \{x_k, -y_k, -\varphi_k\}$, invariance of both the equilibrium distribution and the Smoluchowski operator implies that $\tilde{\Phi}_{l,l'}(q, t) = \tilde{\Phi}_{-l,-l'}(q, t)$. One further checks that $\tilde{\phi}_{l0}^s(q, t) = \mathcal{O}((i v_0^s)^{|l|})$ from checking explicitly the terms $(\Omega^\dagger)^n \exp[i\vec{q} \cdot \vec{r}_s]$ stemming from the expansion of $\exp[\Omega^\dagger t]$, and observing that the non-vanishing angular integrals in $\tilde{\phi}_{l0}^s(q, t)$ require at least the l -fold application of $\delta \Omega^\dagger$.

The low- q expansion of the memory kernel, Eq. (B1), then needs to be combined with the low- q expansion of

$\omega_T^{s,-1}(q)$, Eq. (23), in order to check the leading contributions for the different angular indices. The memory kernels that are relevant for the MSD then read

$$\hat{m}_{00}^s(t) = \frac{nD_t^s}{8\pi} \frac{1}{v_0^s} \int dp \tilde{\phi}_{m'l'}^s(p, t) \times \left\{ -\delta_{|l'|,1} p^3 \tilde{w}_{0,mm'}(p) \tilde{\Phi}_{m0}(p, t) \right\} \quad (\text{B4})$$

and, determining the coupling to the off-diagonal correlator $\hat{\phi}_{\pm 1,0}^s(t)$,

$$\begin{aligned} \hat{m}_{0,\pm 1}^s(t) = & \frac{nD_t^s}{4\pi} \frac{1}{v_0^s} \int dp \tilde{\phi}_{m'l'}^s(p, t) \times \\ & \left\{ iD_t^s p^3 c^s(p)^2 \tilde{\Phi}_{00}(p, t) \delta_{m'0} \delta_{l'0} \right. \\ & + \frac{1}{2} \partial_p p^3 \tilde{w}_{0,mm'}(p) \tilde{\Phi}_{m0}(p, t) \delta_{l'0} \\ & \left. - \frac{D_t^s}{v_0^s} i \delta_{|l'|,1} p^3 \tilde{w}_{0,mm'}(p) \tilde{\Phi}_{m0}(p, t) \right\}. \quad (\text{B5}) \end{aligned}$$

with a memory kernel

$$\hat{m}_{\pm 1,\pm 1}^s(t) = -\frac{nD_t^s}{8\pi} \frac{1}{v_0^s} \int dp \delta_{|1-l'|,1} \tilde{\phi}_{m'l'}^s(p, t) \times p^3 \tilde{w}_{1,mm'}(p) \tilde{\Phi}_{m0}(p, t). \quad (\text{B6})$$

-
- [1] R. Ni, M. A. C. Stuart, and M. Dijkstra, *Nature Commun.* **4**, 2704 (2013).
- [2] A. Liluashvili, J. Ónody, and Th. Voigtmann, *Phys. Rev. E* **96**, 062608 (2017).
- [3] A. Liluashvili and Th. Voigtmann, in *NIC Symposium 2018*, John von Neumann Institute for Computing Series, Vol. 49, edited by K. Binder, M. Müller, and A. Trautmann (Forschungszentrum Jülich, Germany, 2018) pp. 313–320.
- [4] A. Scala, Th. Voigtmann, and C. De Michele, *J. Chem. Phys.* **126**, 134109 (2007).
- [5] J. Reichert and Th. Voigtmann, (2020), in preparation.
- [6] A. L. Thorneywork, S. K. Schnyder, D. G. A. L. Aarts, J. Horbach, R. Roth, and R. P. A. Dullens, *Mol.nPhys.* **116**, 3245 (2018).
- [7] M. Bayer, J. M. Brader, F. Ebert, M. Fuchs, E. Lange, G. Maret, R. Schilling, M. Sperl, and J. P. Wittmer, *Phys. Rev. E* **76**, 011508 (2007).
- [8] F. Weysser, A. M. Puertas, M. Fuchs, and T. Voigtmann, *Phys. Rev. E* **82**, 011504 (2010).
- [9] C. Kurzthaler, S. Leitmann, and T. Franosch, *Sci. Rep.* **6**, 36702 (2016).
- [10] J. Reichert, *Transport Coefficients of dense Active Brownian Particles*, Ph.D. thesis, Heinrich-Heine-Universität Düsseldorf (2020), in preparation.
- [11] T. F. F. Farage and J. M. Brader, [arXiv:1403.0928](https://arxiv.org/abs/1403.0928) (2014).
- [12] S. Mandal, T. Franosch, and Th. Voigtmann, *Soft Matter* **14**, 9153 (2018).
- [13] R. A. Usmani, *Lin. Alg. Appl.* **212/213**, 413 (1994).